Effects of Distance and Driving Force on Photoinduced Electron Transfer between Photosynthetic Reaction Centers and Gold Electrodes

ARTICLE *in* THE JOURNAL OF PHYSICAL CHEMISTRY C · OCTOBER 2007

Impact Factor: 4.77 · DOI: 10.1021/jp0740402

7 AUTHORS, INCLUDING:

Scott Alan Trammell
United States Naval Research Laboratory
72 PUBLICATIONS **2,033** CITATIONS
SEE PROFILE

Igor Griva
George Mason University
43 PUBLICATIONS **342** CITATIONS
SEE PROFILE

Anthony Spano
University of Virginia
27 PUBLICATIONS **743** CITATIONS
SEE PROFILE

Joel M Schnur
George Mason University
115 PUBLICATIONS **3,803** CITATIONS
SEE PROFILE

Effects of Distance and Driving Force on Photoinduced Electron Transfer between Photosynthetic Reaction Centers and Gold Electrodes

Scott A. Trammell,[†] Igor Griva,[‡] Anthony Spano,[§] Stanislav Tsoi,[†] Leonard M. Tender,[†] Joel Schnur,[†] and Nikolai Lebedev*[,†]

Center for Bio/Molecular Sciences & Engineering, U.S. Naval Research Laboratory, Washington, DC 20375, Departments of Mathematical and Computational & Data Sciences, George Mason University, 4400 University Drive, Fairfax, Virginia 22030, and Department of Biology, University of Virginia, Charlottesville, Virginia 22904

Received: May 24, 2007; In Final Form: August 28, 2007

The electron-transfer (ET) parameters for oriented and aligned monolayers of the bacterial photosynthetic reaction center (RC) from *Rhodobacter sphaeroides* formed on the top of self-assembled monolayers (SAMs) of alkanethiols of various lengths immobilized on gold electrode are estimated using cyclic voltammetry and photoelectrochemistry. Utilization of the unique polyHis tag in the protein and the Ni−NTA chelator complex in SAMs allows for specific protein orientation with the RC primary donor facing the electrode. To improve the efficiency of ET between the RC special pair and the electrode, an RC-Cyt complex was formed (*J. Am. Chem. Soc*. **2006**, *128*, 12044−12045). The results are analyzed in terms of integrated Marcus formalism, taking into account the density of electronic states in the metal. The dependence of the ET rate on the distance between RC and electrode demonstrates an adiabatic region up to 10 Å, typical for other proteins, followed by a nonadiabatic area of electron tunneling with a β-factor of ~0.8 per methylene group of the alkanethiol. Reorganization energy of the system is rather low (0.23 eV) and indicates negligible (if any) system conformational change or protein tilting in the course of ET. Scanning probe microscopic (SPM) examination of the constructed surfaces confirmed a high density of surface coverage by the protein and the absence of RC structural deformation in the monolayers. Estimated reduction potential of the RC primary donor for the immobilized protein is +0.5 V (vs NHE), which is close to that observed for the protein in solution and in vivo. These results open the possibility for the measurements and detailed analysis of the mechanisms of ET in photosynthetic proteins in precisely organized monolayers on the surfaces of inorganic electrodes.

Introduction

Understanding the mechanisms of electron-transfer (ET) reactions between photosynthetic proteins and an electrode is of fundamental importance for the construction of bioinspired light energy conversion devices, power sources, chemo- and photosensors, and information processing devices. Among the photoenergetic devices developed by nature, bacterial photosynthetic reaction centers (RCs) are the most efficient. They have a quantum yield of light energy conversion of nearly 100%, an extremely fast operation time for the primary charge separation (about 10^{-9} s or an operation frequency of $\sim 10^9$ Hz), and a highly efficient way of stabilization of separated charges (the ratio of the forward vs back electron-transfer rates is about 10^3).[1,2] These properties make RCs very attractive as possible candidates for the construction of highly efficient bioelectronic and biophotovoltaic devices.[3−5]

RCs are composed of three polypeptides H, L, and M. The polypeptides L and M, each forming five transmembrane α-helices, are arranged in a 2-fold symmetry, whereas the H polypeptide is located at the cytoplasmic surface and binds to both L and M. A dimer of bacteriochlorophylls, the so called primary donor (P), two monomer bacteriochlorophylls (B_A and B_B), two bacteriopheophytins (H_A and H_B), two quinones (Q_A and Q_B), and one iron are all noncovalently bound to the polypeptides and arranged into symmetrical branches.[1,2]

To utilize the advantage of the high efficiency of light energy conversion, the proteins must be immobilized on an electrode. Besides the usefulness for potential engineering applications, the immobilization of protein on electrode provides several scientific benefits as well. First, it allows the identification of protein ET properties in well organized and controlled environments, particularly in protein monolayers. Second, it allows for studying the nonphotochemical ET reactions in the photosynthetic RC (by applying bias voltage to the electrode). Third, it allows for studying the effects of local electric fields generated by the electrode on the ET reactions in- and outside of the protein. Several attempts have been made to immobilize bacterial RC protein on electrodes. Most of them use either nonoriented protein monolayers, or multilayers, or protein incorporated into a nonconductive or low-conductive polymer or lipid matrix.[6−11] In some reports, the protein was oriented to an electrode, but faced the electrode by the top of H-subunit,[4] for which the electron conductive properties are not clear. Meanwhile, to achieve an efficient protein−electrode junction, the oriented and aligned monolayers with close proximity of the protein to electrode would be desirable. Moreover, contrary to some of the other ET proteins,[12−15] information about the ET parameters of photosynthetic RC after its immobilization on electrode surfaces is contradictory.[16] The problem might be due to the

* To whom correspondence should be addressed. E-mail: Nikolai.Lebedev@nrl.navy.mil.
[†] Center for Bio/Molecular Sciences & Engineering.
[‡] Departments of Mathematical and Computational & Data Sciences.
[§] Department of Biology.

10.1021/jp0740402 CCC: $37.00
Published on Web 10/20/2007

SCHEME 1: The Schematic Presentation of Photoinduced and "Dark" Electron Transfers in RC−Cyt−SAM−Gold Electrode

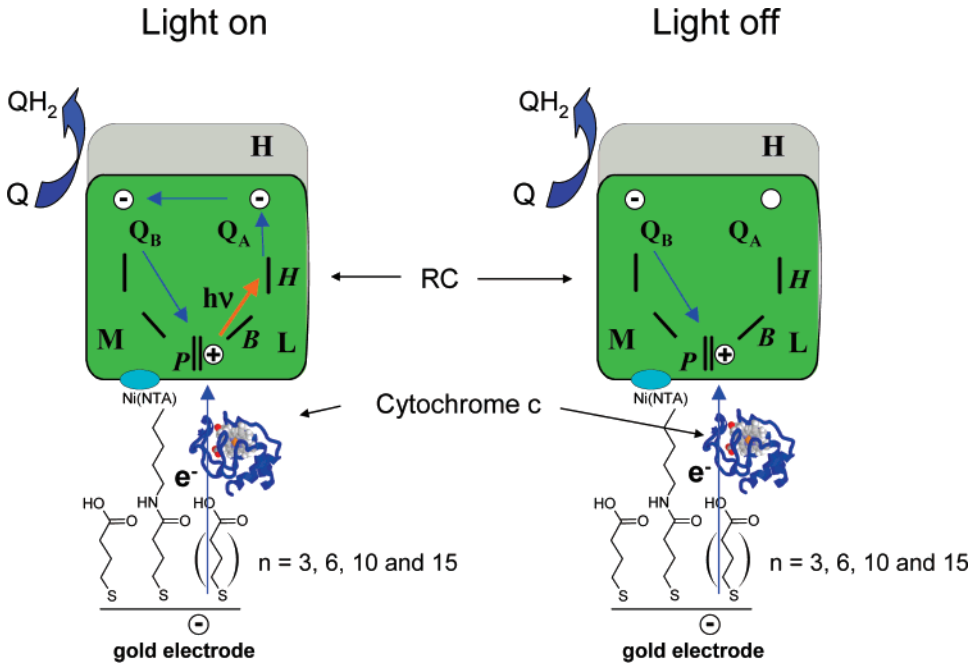

buried location of the electroactive cofactors within the protein globe,[12] the inability of binding the protein in an aligned and oriented way, or the insulating effect of the H-subunit of the protein.[17] Also, since photosynthetic RC is a photoactive protein, the mechanism of its ET reactions might be completely different from those of other electroactive but not photoactive proteins.

Recently, we demonstrated that RC from *Rhodobactor sphaeroides* can be immobilized on gold electrodes modified with a Ni(II) nitrillotriacetic acid (NTA) alkanethiol such that the RC primary electron donor (special pair, P) is orientated toward the electrode surface.[17,18] To accomplish this, we used the RC protein genetically engineered with a polyhistidine tag at the C-terminal end of M-subunit.[19] In the present work, in order to identify the factors controlling photoinduced ET between the immobilized bacterial photosynthetic RC and an underlying electrode, we construct a series of gold electrodes with Ni−NTA-terminated alkanethiol self-assembled monolayers (SAMs) of different thicknesses (3, 6, 10, and 15 methylene units) and immobilized the protein on top of them through a polyHis tag located at the C-terminal end of M-subunit, allowing a specific protein orientation with the primary donor facing the electrode (see Scheme 1). To facilitate ET between the RC special pair and the electrode, cytochrome *c* serving as a conductive wire was incorporated between them.[20] We measured the photocurrent as a function of the applied potential of the working electrode (i.e., driving force) and the distance between the RC and the electrode surface. The results are analyzed in terms of integrated Marcus formalism, taking into account the density of electronic states in the metal. The analysis includes the estimation of midpoint potential of the primary donor, the reorganization energy, and the expected rate constant of electron tunneling between the RC and the electrode. We also try to elucidate the factors that might control the rate of ET on switching the light ON and OFF. Our measurements include (i) the growth to steady-state photocurrent as a function of time (light ON), (ii) the net photocurrent at steady-state conditions, and (iii) the decay of the photocurrent after cessation of illumination (light OFF).

Materials and Methods

Materials. All chemicals were used as received. N_α,N_α-Bis-(carboxymethyl)-L-lysine hydrate (lys−NTA) was obtained from Fluka. 2,3-Dimethoxy-5-methyl-6-geranyl-1,4-benzoquinone (Q2), *N*-(3-dimethylaminopropyl)-*N*-ethylcarbodiimide hydrochloride (EDC), and horse heart cytochrome *c* were obtained from Sigma. 4,4′-Dithiodibutyric acid (linker 1**)** for forming a SAM 3 methylene units thick and 7-carboxyheptyl disulfide acid (linker 2**)** for forming a SAM 6 methylene units thick were obtained from Dojindo Molecular Technologies. 11-Mercaptoundecanoic acid (linker 3) for forming a SAM 10 methylene units thick and 16-mercaptohexadecanoic acid (linker 4) for forming a SAM 15 methylene units thick were obtained from Aldrich. Gold electrodes were obtained from Evaporated Metals Film Corp and consisted of 1 in. long × 3 in. wide × 0.04 in. thick float glass slides coated on one side with a 1000 Å thick gold film over a 50 Å thick chromium adhesion layer. Electrodes were cleaved into approximately 0.2 in. thick sections and cleaned by argon plasma etch (15 min, 200 mTorr, 100 W rf) immediately before use for monolayer preparation.

RC Preparation. The poly histidine tagged RC was expressed and isolated from *Rh. sphaeroides* strain SMpHis constructed by Goldsmith and Boxer (1996).[19] The expression and purification procedure were similar to that described earlier,[17,18] except that after NTA affinity chromatography the protein fraction was subjected to a further round of purification on a Mono-Q anion exchange HPLC column. Fractions containing only the best ratios of A280/A804 (∼1.2) in absorption spectra were collected, pooled, and then dialyzed against 10 mM Tris, pH 8.0, containing 0.05% LDAO. The quality of the RC preparation was confirmed by sodium dodecyl sulfate polyacrylamide gel electrophoresis (SDS-PAGE) (a single band under nondenaturating conditions and three bands of expected molecular weights after protein denaturation), by the protein absorption spectrum (position of the pigment absorption bands and ratios of A278/A804 = 1.26, A760/A804 = 0.38, and A860/A804 = 0.41), and by the kinetics of photoinduced ET within the protein in solution at room temperature under flash excitation

after saturation with quinone (a single exponential recombination reaction between Qb^- and $P860^+$ with a rate constant of about 0.9 s^{-1}). The protein concentration was estimated from the sample absorbance at 804 nm using extinction coefficient 288 mM^{-1} cm^{-1}.[21] The amino acid location in *Rb. sphaeroides* RC structure can be found in Protein Data Base1M3X: 1AIG, 1PCR.

Monolayer Formation. To construct the carboxyl-terminated alkanethiol SAMs of various thicknesses, freshly cleaned gold electrodes were immersed in a 10 mM ethanol solution of one of the carboxyl-terminated alkanethiol compounds overnight and then rinsed with copious amounts of ethanol and deionized (DI) water. To attach NTA to the carboxyl-terminated SAM, each electrode was immersed for 15 min in a 5 mM EDC solution in 100 mM 2-(*N*-morpholino)ethanesulfonic acid (MES) buffer, pH 6.2, rinsed with copious amounts of DI water, immersed for 1 h in a 10 mM lys−NTA in 100 mM potassium phosphate (PB), pH 7.8, rinsed again with copious DI water, and dried under a N_2 stream.

In addition to grafting the NTA to the carboxyl-terminated SAMs, the NTA-terminated monolayers were also formed using the fully intact NTA alkane disulfide, 3,3′-dithiobis[*N*-(5-amino-5-carboxypentyl)propionamide-*N*,*N*′-diacetic acid] dihydrochloride (linker C2-NTA, from Dojindo Molecular Technologies) by exposing the clean gold electrodes to a 1 mM solution of C2-NTA in EtOH overnight.

Efficiency of NTA grafting to the carboxyl-terminated SAMs was determined from the electroactivity of a copper(II)−NTA complex formed on the electrode surface by a reported procedure.[22] For that, a dedicated set of NTA-terminated SAMs using linker 3 was exposed to a 2 mM solution of $CuCl_2$ for 10 min and rinsed with DI water. Electrochemical analysis with cyclic voltammetry (CV) at 100 mV/s in 100 mM potassium phosphate buffer at pH 7 (Ar purged) showed an oxidation of Cu(0) to Cu(II) centered at −0.9 V vs Ag/AgCl after subsequent reduction of the chelated Cu(II) to Cu(0), as reported.[22] Integration of the oxidation peak gave a charge of 16 μC. The coverage, Γ (mol/cm^2), of the Cu−NTA complex was estimated from the relationship $Q = nFA\Gamma$, assuming $n = 2$, and was calculated to be $\sim 0.83 \times 10^{-10}$ mol/cm^2. Electrodes exposed to $CuCl_2$ were not used for the immobilization of protein.

RC Immobilization. The acid groups of the NTA SAMs were deprotonated by immersion of each electrode into a 1 mM aqueous NaOH solution for 15 min followed by rinsing copiously with DI water. The deprotonated NTA SAM terminal groups were bound with Ni^{2+} by immersion of each electrode in a 40 mM aqueous solution of $NiSO_4$ for 15−60 min followed by rinsing with copious DI water and buffer. The polyhistidine tagged RC was immobilized onto the Ni−NTA-terminated SAM by placing a 50−100 μL aliquot of a protein stock solution (0.2 mg/mL in 10 mM phosphate buffer, pH 7.4, 0.05% LDAO) directly onto each electrode at 4 °C in the dark. After incubation with the protein for 1 h, each electrode was rinsed copiously with buffer and immediately used for experiments.

The efficiency of RC binding to the gold electrodes was estimated from the fluorescence analysis of pigments extracted from the surface by 1 mL of cold acetone containing 1−2 μg/mL MgO.[23] Assuming that each protein contains six porphyrins (four bacteriochlorophylls and two bacteriopheophytins), the emission intensity of the pigments at 760 and 785 nm (excitation at 365 nm) was compared to a linear calibration curve of emission intensity vs extracted pigments from protein stock solutions of known concentration. The fluorescence measurements were performed with SPEX Fluorolog-3 spectrofluorometer at room temperature with slit widths equal to 5 nm.

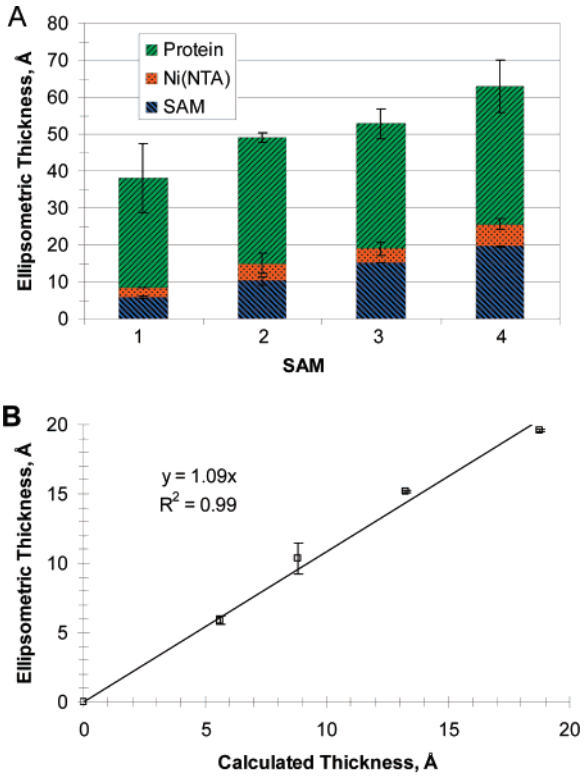

Figure 1. (A) Ellipsometric estimation of the thicknesses of carboxyl-terminated, Ni−NTA-terminated, and RC-terminated alkanethiol SAMs on gold. (B) Correlation between the calculated (from an extended 3D model using Chem3D with a 30° tilt) and the estimated ellipsometric thicknesses of the SAMs on gold. The error bars are ±1 SD from the average of two to three samples.

Ellipsometry. Measurements of monolayer thicknesses on electrodes were performed following each step of the SAM construction procedure (i.e., formation of the carboxyl-terminated alkanethiols, formation of the NTA-terminated alkanethiols, and immobilization of RC) by use of a J. A. Woollam Co. Inc. (Lincoln, NE), multiwavelength ellipsometer with 70 degree contact angle. Freshly cleaned gold electrodes (unmodified) were used for baseline determination. All electrodes were dried with a N_2 stream before each measurement. The ellipsometric data were analyzed assuming an index of fraction of 1.45 for both the monolayer and the protein layers. Expected thicknesses of the carboxyl-terminated SAMs were calculated assuming a simple geometric model with a 30° tilt angle.[24]

Atomic Force Microscopy. Potential flattening of protein upon its immobilization on a SAM-modified gold electrode was tested with tapping mode AFM. Samples for the AFM experiments were prepared using atomically flat gold substrates thermally evaporated on mica. The substrates were functionalized with the linkers C2-NTA and Ni^{2+} as described above and exposed to the RC protein stock solution or RC solution (~0.2 μg/mL) diluted by a factor of 100 at 4 °C for 1 h. Next, the substrates were rinsed with buffer and water and dried under N_2 gas flow. The obtained samples were imaged in air using JEOL SPM-5200 AFM operating in the tapping mode. BudgetSensors Tap300 cantilevers with a force constant of 40 N/m were employed in the measurements.

Cyclic Voltammetry. CV measurements were performed in the dark using a three-electrode configuration with a Model 660 electrochemical workstation (CH Instruments, Austin, TX). A

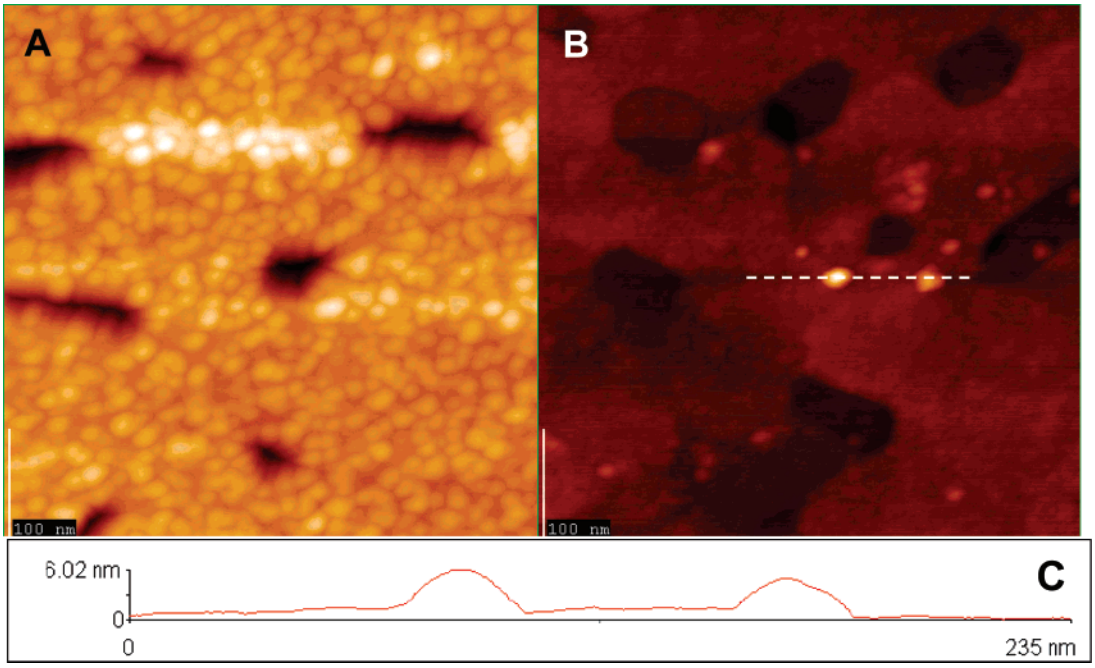

Figure 2. (A) An AFM topographic image of a monolayer of RC proteins on a gold surface modified with the linker C2-NTA. (B) An AFM topographic image of single RC proteins on a C2-NTA-modified gold surface obtained by diluting the original protein solution 100 times. (C) A linear profile along the dashed line in (B) showing the heights of the protein particles. The images were obtained in air using noncontact tapping mode.

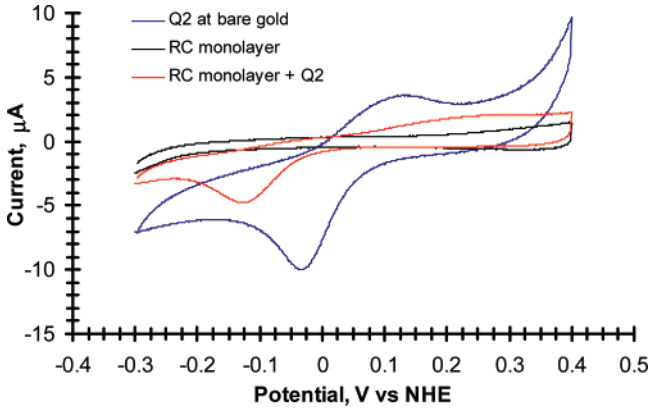

Figure 3. CVs of 40 μM Q2 in solution measured with a bare gold electrode (blue trace) or gold electrode covered with RC protein (red trace). CVs of gold electrode covered with RC protein but without Q2 (black trace). The protein was attached to the electrode through linker 1**.** Experiments were performed in 100 mM Tris buffer at pH 8 in the dark. Scan rate = 20 mV/s.

gold working electrode, a Pt counter electrode, and an Ag/AgCl miniaturized reference electrode[25,26] were used in a one-compartment cell. The experiments were performed in 100 mM Tris buffer (pH 8) or 100 mM potassium phosphate (pH 8). For this paper, we used the IUPAC convention, where positive potentials are plotted in the positive x direction and anodic currents are positive and plotted in the positive y direction.

Photoelectrochemistry. Photocurrents were measured for the RC-modified gold electrodes in 100 mM Tris buffer (pH 8) containing 40 μM Q2 by use of the same three-electrode configuration, electrochemical instrumentation, and electrical contact method described above. The electrodes were arranged in a 3 mL quartz cuvette so that the working electrode could be illuminated by a 150 W xenon lamp equipped with a cutoff filter transmitting wavelengths >700 nm. Light intensity at the electrode surface was measured with a calibrated International Light IL-1700 radiometer and was ~0.1 W/cm^2. This intensity was determined to give a photocurrent near saturation. Photocurrents were recorded for applied potentials of +50, 0, −50, −100, −150, and −200 mV vs the Ag/AgCl miniaturized reference electrode. In the text, all potentials are reported relative to NHE.[27]

The potentials were applied to the RC protein-modified gold electrodes ~5 s before illuminating the cuvette. Photocurrents were recorded for 1−3 s to capture the rising current when the illumination initiated a steady-state current and the decaying current after the illumination terminated. As configured above, the intended electron path is from the underlying electrode to the immobilized RC via tunneling across the intervening SAM to the RC primary donor and eventually to Q2 in solution. Photocurrent measured as a function of Q2 concentration indicated that the photocurrent is independent of Q2 concentration above 20 μM. Photocurrent time profiles were collected at a resolution of 5 ms, corrected for a baseline drift, and smoothed using software supplied with the potentiostat. An example is shown in the Supporting Information.

Estimation of Reorganization Energy. The experimental data were treated in accordance to the Marcus voltage-electron-transfer rate expression taking into account density of electronic states of the electrodes.[28,29] Following Tender et al.,[29] the pertinent equations are:

$$i_{ss,\eta,d} = nFAk_{ss,\eta,n}\Gamma_{RC^*} \quad (1)$$

$$k_{ss,\eta,d} = k_{ox,,\eta,d} - k_{red,\eta,d} \quad (2)$$

$$\eta = E_{app} - E_{mp} \quad (3)$$

$$k_{red,\eta,d} = \mu\rho k_B T \sum_{x=-100}^{100}\left[\frac{\exp\{-(x-(\lambda+\eta)/k_BT)^2(k_BT/4\lambda)\}}{1+\exp(x)}\right] \quad (4)$$

$$k_{ox,\eta,d} = \mu\rho k_B T \sum_{x=-100}^{100}\left[\frac{\exp\{-(x-(\lambda+\eta)/k_BT)^2(k_BT/4\lambda)\}}{1+\exp(x)}\right] \quad (5)$$

$$\mu = \mu_o \exp(-\beta d) \quad (6)$$

where $i_{ss,\eta,d}$ is the steady-state photocurrent for a given overpotential (η) and SAM thickness (d), n is the number of electrons transferred per RC per reaction event ($n = 1$), F the Faraday constant ($F = 96\,487$ C/mol e$^-$), A is the electrode area ($A = 1$ cm^2), Γ_{RC*} is the surface density of RC contributing to steady-state photocurrent, E_{app} is the potential applied to the electrode, E_{mp} is the midpoint (formal potential) of the cofactor (i.e., cytochrome c or the primary donor) directly exchanging electrons with the electrode, $k_{ss,\eta,n}$ is the η- and d-dependent net rate of electron transfer between Q2 in solution and the electrode via RC-mediated electron transfer, $k_{ox,,\eta,d}$ is the η- and d-dependent rate of electron transfer from Q2 to the electrode via RC-mediated electron transfer contributing to $k_{ss,\eta,n}$, $k_{red,\eta,d}$ is the η- and d-dependent rate of electron transfer from the electrode to Q2 via RC-mediated electron transfer contributing to $k_{ss,\eta,n}$, λ is the electron-transfer reorganization energy barrier, μ is the distance-dependent overlap or coupling between the electronic orbitals of the electrode and the cofactor directly exchanging electrons with the electrode, ρ is the density of electronic states of the electrode, $\mu°$ is the orbital coupling at zero distance separating the cofactor and the electrode, and x is electron energy relative to the Fermi level. It is important to note here that the observed photocurrent is cathodic (i.e., $i_{ss,\eta,d}$ and $k_{ss,\eta,n}$ are <0) indicating a net transfer of electrons from the electrode.

For estimation of the reorganization energy (λ) from experimental data, we approximate the ET rate constant k_η by the discrete sums as described above and then minimize the deviation of the rate constants $k_\eta(\lambda)$ as a function of λ from the measured rate constants $\bar{k}_\eta$ as

$$\lim_{\lambda} \sum_{\eta} (k_\eta(\lambda) - \bar{k}_\eta)^2 \quad (7)$$

Minimization is done by Newton's method using modified software LOQO.[30]

Results and Discussion

Construction and Characterization of SAMs. SAMs of alkane linkers of 3, 6, 10, and 15 methylene units long containing terminal nitrillotriacetic acid (NTA) groups at the end were used for oriented immobilization of RC on gold electrodes.[17,18] The NTA groups on the monolayer bind RC through a genetically engineered polyhistidine tag located at the C-terminal end of the protein M-subunit at close proximity to the RC primary donor (special pair, P, Scheme 1). Ellipsometry was used to monitor the SAM thickness of selected electrodes following progression from the carboxyl-terminated to the NTA-terminated to the RC-bound SAMs assuming a 30° tilt for the alkane chain.[31−33] The results demonstrate excellent correlation between predicted and observed thicknesses (Figure 1), consistent with a set of well-ordered SAMs of thickness that is linearly dependent on the number of methylene units within the alkanethiol used, and show nearly 100% of surface coverage. At this coverage, the average distance between the alkane chains on the surface is about 5 Å.[34] These results are consistent with a set of relatively well-ordered carboxyl-terminated SAMs of thickness that is linearly dependent on the number methylene units within the alkanethiol used. Thicknesses determined by ellipsometery after conversion of the carboxyl-terminated SAMs to Ni−NTA-terminated SAMs increased by 3−6 Å, which is consistent with a recent report on the thickness of the Ni−NTA groups in similar grafting procedures using carboxyl-terminated alkane SAMs.[35]

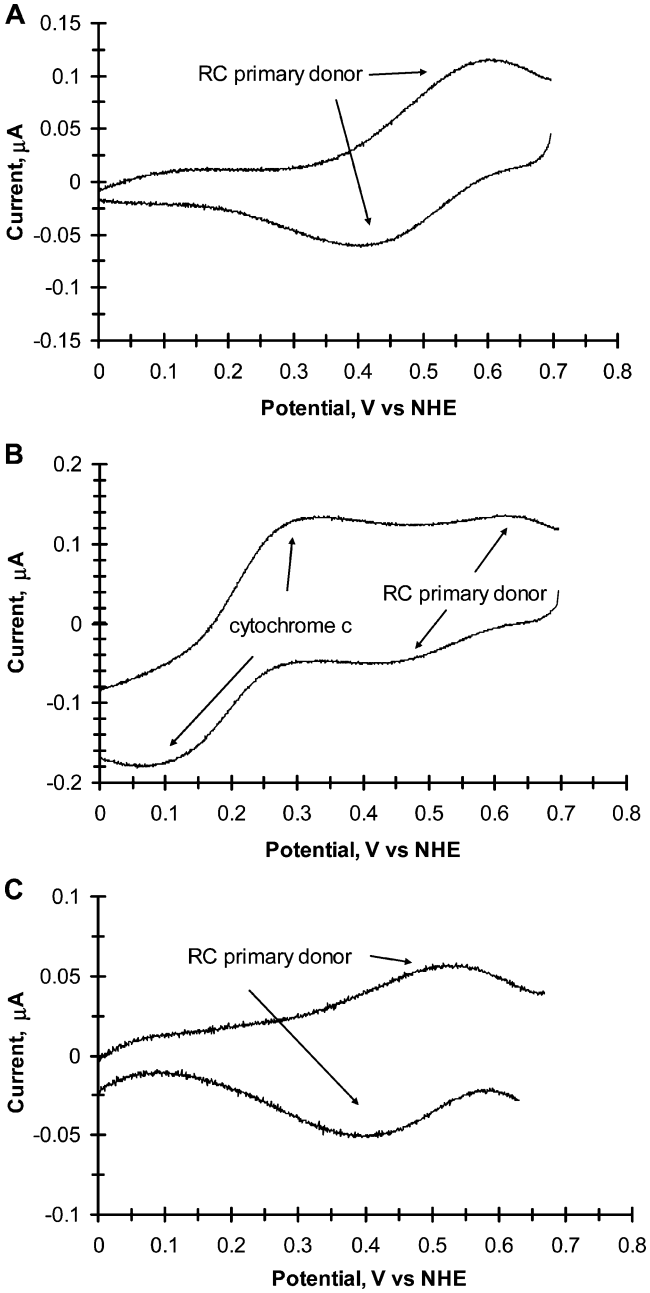

Figure 4. (A) Background subtracted CV of a RC-modified electrode. (B) Background subtracted CV of a RC-modified electrode after addition of 10 μM cytochrome c to the electrolyte. (C) Background subtracted CV of a RC-modified electrode after exposure to 10 μM cytochrome c and subsequent rinsing with buffer. Electrolyte = 100 mM potassium phosphate buffer, pH 8. Scan rate = 20 mV/s.

Estimation of Protein Coverage and Size. After RC immobilization on the top of the linker SAMs, the thicknesses of the monolayers increased by 30−34 Å (Figure 1). This is lower than one might expect for a protein having a size of about 60−67 Å, as estimated by crystallographic analysis.[36] This decrease might be due to either protein flattening (denaturing due to the absence of water) on the electrode or incomplete coverage of the surface by the protein. To test the first possibility, we constructed similar SAMs from the linker C2-NTA and exposed them to either the same (Figure 2A) or the lower protein concentrations (diluted to 1/100, Figure 2B) to examine individual proteins on the top of the SAM with a

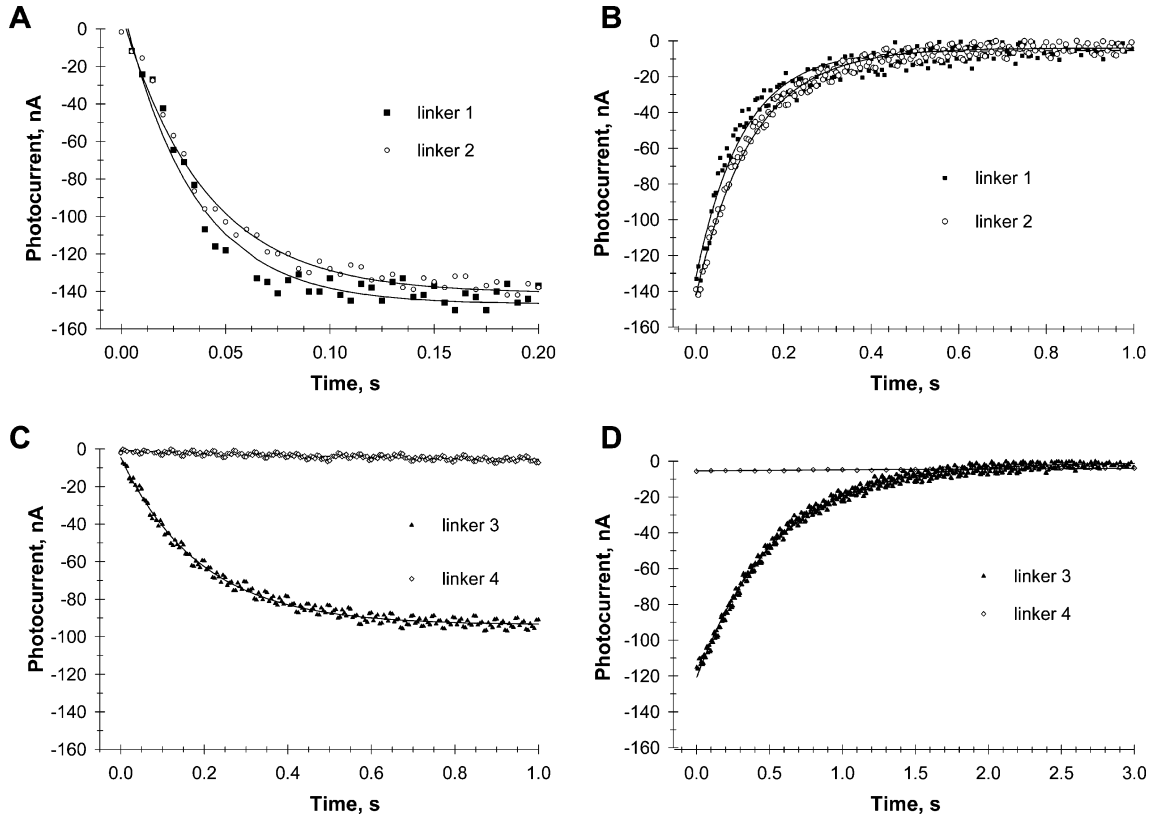

Figure 5. Kinetics of the photocurrent at switching light ON (A) and OFF (B) observed with RC-modified gold electrodes using linkers 1 and 2. Kinetics observed with linkers 3 and 4 at switching light ON (C) and OFF (D). An electrode potential of +0.10 V was applied to the electrode about 5 s before and maintained 5 s after illumination (>700 nm). The electrolyte was 0.1 M Tris buffer, pH 8, with 40 μM Q2. The data were fit with single exponential growth and decays with rate constants listed in Table 1.

tapping mode AFM.[37,38] The topographic image of a surface formed with diluted RC reveals the presence of individual particles with height ~6 nm over the linker monolayer (Figure 2C). This size is typical for RC protein. Thus, the lower thickness of the protein monolayer observed in ellipsometric experiments is more likely due to incomplete coverage of the electrode surface by the protein. This conclusion is not in contradiction with the image of the protein monolayer in Figure 2A in view of the broadening of single proteins in the AFM image caused by the finite size of the apex of the cantilever tip. It is consistent with the estimation of RC surface density from the fluorescence analysis of pigments extracted from the surfaces, which shows a surface density of RC per unit area of $\sim 3 \times 10^{-12}$ mol/cm^2.

Estimation of the Midpoint Potential of ET Cofactors at the RC−Gold Electrode in the Dark. To ensure stable electrical connection between electrodes in the constructed electrochemical cells, two ET mediators were added, namely, Q2 and cytochrome *c*.[17,18] Q2 is an electron acceptor and the reduced cytrochrome *c* is an electron donor for electrode immobilized RC in photoelectrochemical experiments.[39] These mediators can potentially directly interact with the working electrode. In order to determine their possible contributions to photocurrent and the midpoint potentials of these compounds, cyclic voltammograms (CV) were recorded for various combinations of these cofactors with and without immobilized RC in near dark conditions.

Figure 3 depicts voltammograms for 40 μM Q2 in the electrolyte at a freshly cleaned bare gold electrode (i.e., no SAM or RC) and at gold electrode covered with RC immobilized by using linker 1**.** A CV for RC-covered electrode without Q2 in solution is also shown for comparison. These voltammograms indicate that Q2 is electroactive with a midpoint potential of ~0.05 V vs NHE at bare gold. At the same time, immobilized RC is electroinactive without Q2 and cytochrome *c* in the examined potential region in the dark. These voltammograms also indicate that the SAM and immobilized RC substantially block the background current between Q2 and electrode.[39−42]

Cyclic voltammograms over a more oxidizing voltage region for a gold electrode modified with linker C2-NTA before and after immobilization of RC reveal an additional redox couple due to immobilized RC. To help with the analysis, the CVs were background subtracted and the baselines corrected (see Supporting Information). A resultant CV is shown in Figure 4A. For immobilized photosynthetic RCs, we observe a reversible redox couple at +0.5 V (vs NHE), which is similar to that estimated for the RC primary donor (special pair) by redox titration with optical monitoring for isolated RC in solutions and in vivo.[43−49] This result indicates that the RC does not change its redox properties upon binding to gold throughNi−NTA alkanethiol linkers. Integration of the both anodic and cathodic peaks in the CVs gives $\sim 4 \times 10^{-12}$ mol/cm^2 of RC coverage, which is within experimental error of the estimate from the fluorescence analysis. In addition, at the slow scan rate of 20 mV/s, a large peak-to-peak separation between the anodic and cathodic peaks (~0.19 V) was observed suggesting slow electron transfer between the electrode and the primary donor in the protein. This is consistent with the fact that the primary donor is slightly buried within the protein, as measured in the X-ray crystal structure of the protein (~11 Å from the primary donor (special pair) to the protein surface around Tyr162).[20]

Figure 4B depicts a background subtracted voltammogram for a gold electrode modified with RC after the addition of 40

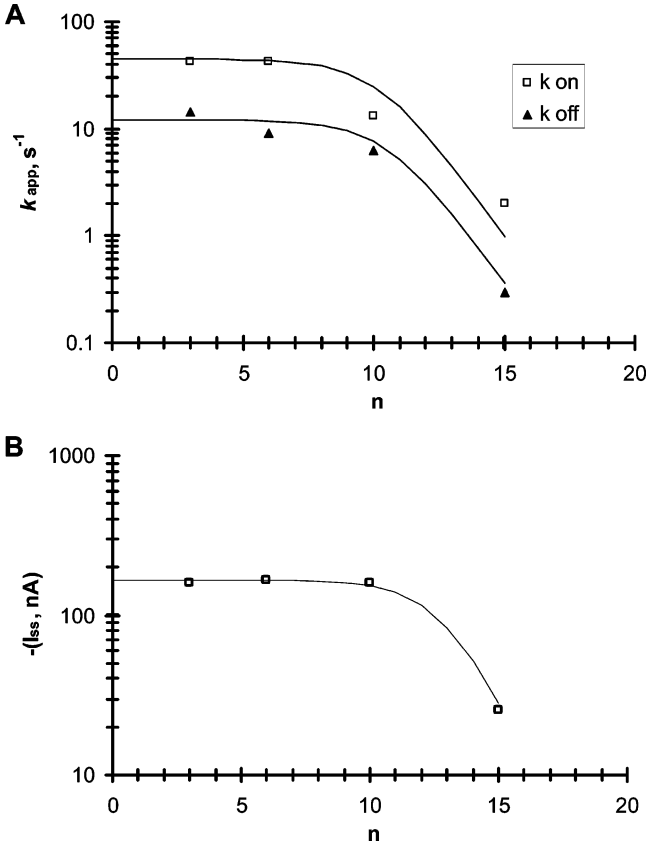

Figure 6. (A) Dependence of the rate of photocurrent increase at the beginning of illumination (light ON, □**)** and the rate of photocurrent decay at the cessation of illumination (light OFF, ▲**)** on the distance between RC and electrode (SAM thickness). (B) Dependence of the steady-state photocurrent on the distance between RC and gold electrode at 0 V vs NHE. In all experiments the electrolyte was 0.1 M Tris buffer, pH 8, with 40 μM Q2. The illumination was done with IR light (>700 nm) at saturated intensities (0.1 W cm^{-2} at the electrode surface). The fitted lines represent a calculation using eq 10 with $\beta = 0.8$ and $k_{lim} =$ 43 s^{-1} for light ON and $k_{lim} = 12$ s^{-1} for light OFF.

μM cytochrome *c* in the electrolyte. The voltammogram indicates that cytochrome *c* is electroactive at the SAM-modified electrodes with immobilized RC. In addition, the midpoint potential at +0.2 V is consistent with reported results of cytochrome *c* at carboxyl-terminated SAMs.[50,51] These CV waves completely disappear after washing out cytochrome from the electrolyte. Figure 4C shows a background subtracted voltammogram of the same RC-modified electrode after exposure to cytochrome *c* and with subsequent rinsing with buffer. In this sample, only the redox couple of the primary donor can be seen. Moreover, it shifts by −30 mV to 0.47 V vs NHE suggesting the change of RC primary donor redox potential after the formation of the complex with cytochrome. Also, the peak-to-peak separation of the anodic and cathodic peaks decreases to 0.13 V, signifying an increase in the rate of electron transfer between RC and electrode consistent with the results obtained earlier.[20]

Photoinduced ET Between the Immobilized RC and Gold Electrode. Figure 5 contains kinetic traces of photocurrent at an applied potential +0.10 V (vs NHE) for RC immobilized on gold electrodes after exposure to cytochrome *c* and with Q2 in solution. For each record, the potential was applied ~10 s before illumination and the measurements were made to capture the kinetics of current rising at the beginning of illumination (ON rate), a steady-state current, and the current decay after cessation of illumination (OFF rate). For these experiments, the light wavelength was >700 nm and the intensity was clos to saturation (0.1 W cm^{-2} at the electrode surface). The photocurrent was stable and would repeat with high fidelity. Examination of the photocurrent shows that the kinetics of photocurrent changes at each applied potential can be fit to a single exponential curve:

$$i(t)_{on} = i_{ss}\,(1 - \exp(-k_{on}t)) \tag{8}$$

$$i(t)_{off} = i_{ss}\exp(-k_{off}t) \tag{9}$$

where $i(t)$ is the time-dependent photocurrent for a given applied voltage and SAM thickness, and k_{on} and k_{off} are rate constants for the rising photocurrent (when illumination initiated) and the decaying photocurrent (when illumination terminated), respectively, for a given applied voltage and SAM thickness.

The results show a dramatic dependence of the photocurrent on linker lengths. Figure 6 contains plots of the steady-state photocurrent and ON and OFF rate constants vs distance to electrode for a series of RC-modified gold electrodes. In addition, a considerable difference between the ON and OFF photocurrent rates is also shown, possibly reflecting different recombination rates within RC between an illuminated and dark state.

In all cases, two functional areas are clearly seen. At short distance to the electrode (about 10 Å), the current (or rate constant) is nearly independent of the distance (adiabatic area). At longer distances, it substantially decreases. The observed kinetic rate constants (k_{on} or k_{off}) can be fit to the reciprocal relationship (eq 10)[52] with two terms corresponding to (i) the electron exchange (k_{ET}) between the electrode and RC and (ii) a rate-limiting step associated within the system.

$$1/k_{on} \text{ or } 1/k_{off} = 1/k_{ET} + 1/k_{lim} \tag{10a}$$

$$1/I_{ss} = 1/I_{ET} + 1/I_{lim} \tag{10b}$$

For protein immobilized on an electrode, at low applied potentials and long distances between the protein and electrode, the ET is mainly controlled by the overlapping of electronic wavefunctions and depends exponentially on the distance between RC and electrode:[46−49]

$$k_{ET} = k_o \exp(-\beta n) \tag{11a}$$

$$I_{ET} = I_o \exp(-\beta n) \tag{11b}$$

where k_{ET} is the steady-state rate (or current *I*ss) of ET for a given applied voltage at a given SAM thickness, k_o is the rate (or current I_o) at zero distance, β is the distance-dependence parameter (tunneling attenuation factor), and *n* is the distance between the protein and electrode expressed in number of methylene units in the linker. Analysis of the decay of ET on the distance to electrode for the linkers with 10 and 15 methylene units gives distance-dependence factor for ET RC to gold, $\beta = 0.8$ per methylene unit (Table 1), that is close to typical values for alkanethiol SAMs.[12−14,49] Extrapolation of this dependence to the zero distance gives the maximal rate constant for electron tunneling between flat gold electrode and special pair in RC−cytochrome complex about ($k_o = 10^4$−10^5 s^{-1}).

Among the factors that can eliminate the rate of ET for immobilized RC at short distances to electrode might be charge transfer within the protein or between the protein and the electrode. Within RC, the slowest steps for forward ET are between quinones Q_a and Q_b (~0.1 ms, $k = 10^4$ s^{-1}), proton

TABLE 1: Transition Rates (k) and RC Reorganization Energies (λ) Estimated from the Transient Kinetics of Photocurrent between RC and Gold Electrode at the Onset of Illumination (k_{on}), at Cessation of Illumination (k_{off}), and from the Steady-State Photocurrent (I_{ss}) at Various Electrode Potentials (vs NHE) and Linker Lengths (L) Assuming a Normal Midpoint Potential of the Special Pair (+0.47 V vs NHE

	L = 3 methylene units			L = 6 methylene units			L = 10 methylene units			L = 15 methylene units		
electrode potential (V vs NHE)	k_{on} (s^{-1})	k_{off} (s^{-1})	I_{ss} (nA/cm^2)	k_{on} (s^{-1})	k_{off} (s^{-1})	I_{ss} (nA/cm^2)	k_{on} (s^{-1})	k_{off} (s^{-1})	I_{ss} (nA/cm^2)	k_{on} (s^{-1})	k_{off} (s^{-1})	I_{ss} (nA/cm^2)
0	43	14.4	−161	43	9.1	−167	13	6.3	−158.5	2	0.3	−25.3
0.05	42	12.3	−148	34	9.6	−133	8.6	3.7	−114	1.8	0.08	−11.7
0.1	41	11.7	−129	31.6	8.2	−94	7.5	1.9	−82	1.5		−5.3
0.15	40.5	7.4	−109	21.9	6.6	−74	4	1	−48.5			−2
0.2	28	4.5	−68	17.2	4.8	−43	3	0.59	−26.5			−0.5
0.25	8		−25	15.8	3.1	−14.5		0.38	−10			0
λ (eV)	0.21	0.23	0.23	0.21	0.21	0.25	0.23	0.25	0.28	n/a	n/a	0.64
error (%)	14	4.7	0.18	11.7	2.9	0.15	3.5	1.2	0.12	n/a	n/a	0.01

transfer to Q_b (~0.2 ms, $k = 5 \times 10^3\ s^{-1}$), and Q_b dissociation from the protein (~25 ms, $k = 40\ s^{-1}$) (see scheme).[21,53−55] For recombination of the photoseparated charges (back reaction), the slowest steps for ET are from the primary quinone (Q_a) to P^+ (~0.1 s, $k = 10\ s^{-1}$) and from the secondary quinone (Q_b) to P^+ (1−5 s, $k = 0.2-1\ s^{-1}$).[21,53−55] As depicted in plot A of Figure 6, k_{on} shows an apparent limit at 43 s^{-1} and k_{off} appears to be limited to 12 s^{-1}. These rates are similar to the rates of reduced secondary quinone (Q_b) dissociation from RC protein and ET from the reduced primary quinone (Q_a) to the oxidized special pair (P^+), respectively.[21,53−55] Our estimates of the recombination rate constants between Q_a and P^+ for our RC preparations in solution using photoinduced differential absorption spectroscopy[53,55] show similar values (8 s^{-1}, data not shown).

Estimation of Reorganization Energy of Bacterial Photosynthetic RC upon ET on Gold Electrode. The RC protein is known to have a rather rigid structure that can operate in frozen solutions[1,2,21] and in solid-state devices.[55] To estimate the reorganization energy, we measured ON, OFF, and steady-state ET rates for RC sitting on SAMs of different thicknesses at various potentials of the working electrode. Calculations were performed by fitting Marcus' model integrated over the density of electronic states of gold electrode[28,29] into the experimental data, assuming the normal midpoint potential of the primary donor (E_m) is equal to +0.47 V. For short distances and reducing conditions, the results show consistent low reorganization energy ($\lambda = 0.21-0.23$ eV) for ON, OFF, and steady-state photocurrent (Table 1). This low λ is similar to that estimated for ET within the protein in solution by differential absorption spectroscopy[46−49] and confirms that the protein−short linker−electrode complexes have rigid structures and do not undergo substantial conformational changes in the course of ET. At longer distances from the electrode, considerable increase in λ was observed (Table 1) that could be due to linker mobility and/or protein tilting.

Conclusions

Our results show that well organized oriented and aligned monolayers of bacterial photosynthetic reaction center proteins on gold electrode can be self-assembled using NTA-terminated alkanethiol bridges. After the immobilization, the photosynthetic RC retains its shape and the main ET properties, including its ability for photoinduced ET, and has a normal midpoint potential of the primary donor (+0.5 V) similar to those determined by differential absorption spectroscopy in solution and in vivo. In the presence of cytochrome *c*, the assembled gold−SAM−NTA−RC−cyt complexes possess low reorganization energy (0.23 eV) in the course of ET and thus can be used for the construction of solid-state photovoltaic devices. The distance-dependence factor of electron tunneling for RC immobilized with alkane bridges is equal to 0.8 per methylene unit, similar to that reported for these bridges in other systems. This indicates the importance of close location of the protein to electrode for achieving efficient RC−electrode junction. Analysis of the dependence of the ET rate on the distance to the electrode demonstrates that the constructed surfaces have an adiabatic area of about 10−12 Å. Estimated by extrapolation from the nonadiabatic area, the maximal tunneling rate constant for ET from the flat gold electrode to RC primary donor is about $10^4-10^5\ s^{-1}$. Our on going efforts include identification and remediation of the rate-limiting steps to make more efficient solid-state photovoltaic devices.

Acknowledgment. The authors are grateful to Benjamin Goodman (Johns Hopkins University) and Joe McDermott (Carnegie Mellon University) for their help with molecular biological and electrochemical experiments while they were with the University of Virginia and with Naval Research Laboratory, respectively. This work was supported in parts by DARPA (N.L. and I.G.), AFOSR (N.L.), and the Office of Naval Research via the NRL base program (N.L. and S.A.T.).

Supporting Information Available: Cyclic voltammogram data, table of ellipsometric data, and photocurrent time profiles with and without smoothing. This material is available free of charge via the Internet at http://pubs.acs.org.

References and Notes

(1) Hoff, A. J.; Deisenhofer, J. *Phys. Rep.* **1997**, *287*, 2−247.
(2) Sundstrom, V. *Prog. Quantum Electron.* **2000**, *24*, 187−238.
(3) Lee, I.; Lee, J. W.; Greenbaum, E. *Phys. Rev. Lett.* **1997**, *79*, 3294−3297.
(4) Nakamura, C.; Hasegawa, M.; Yasuda, Y.; Miyake, J. *Appl. Biochem. Biotechnol.* **2000**, *84*−*6*, 401−408.
(5) Das, R.; Kiley, P. J.; Segal, M.; Norville, J.; Yu, A. A.; Wang, L. Y.; Trammell, S. A.; Reddick, L. E.; Kumar, R.; Stellacci, F.; Lebedev, N.; Schnur, J.; Bruce, B. D.; Zhang, S. G.; Baldo, M. *Nano Lett.* **2004**, *4*, 1079−1083.
(6) Kong, J. L.; Sun, W. L.; Wu, X. L.; Deng, J. Q.; Lu, Z. Q.; Lvov, Y.; Desamero, R. Z. B.; Frank, H. A.; Rusling, J. F. *Bioelectrochem. Bioenerg.* **1999**, *48*, 101−107.
(7) Cao, Y. B.; Chen, D. D.; Wu, X. L.; Kong, J. L.; Zou, Y. L.; Xu, C. H. *Anal. Lett.* **2001**, *34*, 713−725.
(8) Matsumoto, K.; Fujioka, S.; Mii, Y.; Wada, M.; Erabi, T. *Electrochemistry* **2001**, *69*, 340−343.
(9) Zhao, J. Q.; Ma, N.; Liu, B. H.; Zhou, Y. L.; Xu, C. H.; Kong, J. L. *J. Photochem. Photobiol., A* **2002**, *152*, 53−60.
(10) Zhao, J. Q.; Liu, B. H.; Zou, Y. L.; Xu, C. H.; Kong, J. L. *Electrochim. Acta* **2002**, *47*, 2013−2017.
(11) Munge, B.; Das, S. K.; Ilagan, R.; Pendon, Z.; Yang, J.; Frank, H. A.; Rusling, J. F. *J. Am. Chem. Soc.* **2003**, *125*, 12457−12463.
(12) Jeuken, L. J. C.; Jones, A. K.; Chapman, S. K.; Cecchini, G.; Armstrong, F. A. *J. Am. Chem. Soc.* **2002**, *124*, 5702−5713.

(13) Khoshtariya, D. E.; Wei, J. J.; Liu, H. Y.; Yue, H. J.; Waldeck, D. H. *J. Am. Chem. Soc.* **2003**, *125*, 7704−7714.
(14) Murgida, D. H.; Hildebrandt, P. *Acc. Chem. Res.* **2004**, *37*, 854−861.
(15) Haas, A. S.; Pilloud, D. L.; Reddy, K. S.; Babcock, G. T.; Moser, C. C.; Blasie, J. K.; Dutton, P. L. *J. Phys. Chem. B.* **2001**, *105*, 11351−11362.
(16) Willner, I.; Willner, B. *Coord. Chem. Rev.* **2003**, *245*, 139−151.
(17) Trammell, S. A.; Spano, A.; Price, R.; Lebedev, N. *Biosens. Bioelectron.* **2006**, *21*, 1023−1028.
(18) Trammell, S. A.; Wang, L. Y.; Zullo, J. M.; Shashidhar, R.; Lebedev, N. *Biosens. Bioelectron.* **2004**, *19*, 1649−1655.
(19) Goldsmith, J. O.; Boxer, S. G. *Biochim. Biophys. Acta* **1996**, *1276*, 171−175.
(20) Lebedev, N.; Trammell, S. A.; Spano, A.; Lukashev, E.; Griva, I.; Schnur, J. *J. Am. Chem. Soc.* **2006**, *128*, 12044−12045.
(21) Kleinfeld, D.; Okamura, M. Y.; Feher, G. *Biochemistry* **1984**, *23*, 5780−5786.
(22) Blankespoor, R.; Limoges, B.; Schollhorn, B.; Syssa-Magale, J. L.; Yazidi, D. *Langmuir* **2005**, *21*, 3362−3375.
(23) Lebedev, N.; Timko, M. P. *Photosynth. Res.* **2002**, *74*, 153−163.
(24) Bain, C. D.; Troughton, E. B.; Tao, Y. T.; Evall, J.; Whitesides, G. M.; Nuzzo, R. G. *J. Am. Chem. Soc.* **1989**, *111*, 321−335.
(25) Ciobanu, M.; Wilburn, J. P.; Lowy, D. A. *Electroanalysis* **2004**, *16*, 1351−1358.
(26) Ciobanu, M.; Wilburn, J. R.; Buss, N. L.; Ditavong, P.; Lowy, D. A. *Electroanalysis* **2002**, *14*, 989−997.
(27) Bard, A. J.; Larry, R. F. *Electrochemical methods: fundamentals and applications*, 2nd ed.; Wiley: New York, 2001.
(28) Chidsey, C. E. D. *Science* **1991**, *251*, 919−922.
(29) Tender, L.; Carter, M. T.; Murray, R. W. *Anal. Chem.* **1994**, *66*, 3173−3181.
(30) Griva, I. *Comput. Optim. Appl.* **2004**, *29*, 173−195.
(31) Sigal, G. B.; Bamdad, C.; Barberis, A.; Strominger, J.; Whitesides, G. M. *Anal. Chem.* **1996**, *68*, 490−497.
(32) Ferretti, S.; Paynter, S.; Russell, D. A.; Sapsford, K. E.; Richardson, D. J. *Trends Anal. Chem.* **2000**, *19*, 530−540.
(33) Flink, S.; van Veggel, F.; Reinhoudt, D. N. *Adv. Mater.* **2000**, *12*, 1315−1328.
(34) Strong, L.; Whitesides, G. M. *Langmuir* **1988**, *4*, 546−558.
(35) Lee, J. K.; Kim, Y. G.; Chi, Y. S.; Yun, W. S.; Choi, I. S. *J. Phys. Chem. B* **2004**, *108*, 7665−7673.
(36) Allen, J. P.; Feher, G.; Yeates, T. O.; Komiya, H.; Rees, D. C. *Proc. Natl. Acad. Sci. U.S.A.* **1987**, *84*, 6162−6166.
(37) Fotiadis, D.; Scheuring, S.; Muller, S. A.; Engel, A.; Muller, D. J. *Micron* **2002**, *33*, 385−397.
(38) Scheuring, S.; Seguin, J.; Marco, S.; Levy, D.; Robert, B.; Rigaud, J. L. *Proc. Natl. Acad. Sci. U.S.A.* **2003**, *100*, 1690−1693.
(39) Katz, E. Y.; Shkuropatov, A. Y.; Vagabova, O. I.; Shuvalov, V. A. *Biochim. Biophys. Acta* **1989**, *976*, 121−128.
(40) Sato, Y.; Fujita, M.; Mizutani, F.; Uosaki, K. *J. Electroanal. Chem.* **1996**, *409*, 145−154.
(41) Yousaf, M. N.; Mrksich, M. *J. Am. Chem. Soc.* **1999**, *121*, 4286−4287.
(42) Budavari, V.; Szucs, A.; Somlai, C.; Novak, M. *Electrochim. Acta* **2002**, *47*, 4351−4356.
(43) Lin, X.; Murchison, H. A.; Nagarajan, V.; Parson, W. W.; Allen, J. P.; Williams, J. C. *Proc. Natl. Acad. Sci. U.S.A.* **1994**, *91*, 10265−10269.
(44) Hara, M.; Asada, Y.; Miyake, J. *Mater. Sci. Eng., C* **1997**, *4*, 321−325.
(45) Munge, B.; Pendon, Z.; Frank, H. A.; Rusling, J. F. *Bioelectrochemistry* **2001**, *54*, 145−150.
(46) Marcus, R. A.; Sutin, N. *Biochim. Biophys. Acta* **1985**, *811*, 265−322.
(47) Beratan, D. N.; Betts, J. N.; Onuchic, J. N. *J. Phys. Chem.* **1992**, *96*, 2852−2855.
(48) Arnaut, L. G.; Formosinho, S. J. *J. Photochem. Photobiol., A.* **1997**, *111*, 111−138.
(49) Page, C. C.; Moser, C. C.; Chen, X. X.; Dutton, P. L. *Nature* **1999**, *402*, 47−52.
(50) Chen, X. X.; Ferrigno, R.; Yang, J.; Whitesides, G. A. *Langmuir* **2002**, *18*, 7009−7015.
(51) Tarlov, M. J.; Bowden, E. F. *J. Am. Chem. Soc.* **1991**, *113*, 1847−1849.
(52) Armstrong, F. A. Applications of voltammetric methods for probing the chemistry of redox proteins. In *Bioelectrochemistry of biomacromolecules*; Lenaz, G., Milazzo, G., Eds.; Birkhāuser Verlag: Boston, 1997; p 205.
(53) Xu, Q.; Gunner, M. R. *Biochemistry* **2001**, *40*, 3232−3241.
(54) Paddock, M. L.; Adelroth, P.; Feher, G.; Okamura, M. Y.; Beatty, J. T. *Biochemistry* **2002**, *41*, 14716−14725.
(55) Milano, F.; Agostiano, A.; Mavelli, F.; Trotta, M. *Eur. J. Biochem.* **2003**, *270*, 4595−4605.